Title: Hierarchical Unsupervised Change Detection in Multitemporal Hyperspectral Images

This paper appears in: IEEE Transactions on Geoscience and Remote Sensing

Date of Publication: 29 May, 2014

Author(s): Sicong Liu, Lorenzo Bruzzone, Francesca Bovolo, and Peijun Du

Volume:

Page(s):

DOI: 10.1109/TGRS.2014.2321277

HIERARCHICAL UNSUPERVISED CHANGE DETECTION IN MULTITEMPORAL HYPERSPECTRAL IMAGES

Sicong Liu, *Student Member*, *IEEE*, Lorenzo Bruzzone, *Fellow*, *IEEE*, Francesca Bovolo, *Senior Member*, *IEEE*, and Peijun Du, *Senior Member*, *IEEE*

ABSTRACT

The new generation of satellite hyperspectral sensors can acquire very detailed spectral information directly related to land surface materials. Thus when multitemporal images are considered, they allow us to detect many potential changes in land covers. This paper addresses the change detection problem in multitemporal hyperspectral remote sensing images, analyzing the complexity of this task. A novel hierarchical change-detection approach is proposed, which is aimed to identify all the possible change classes present between the considered images. In greater detail, in order to formalize the change-detection problem in hyperspectral images, an analysis of the concept of "change" is given from the perspective of pixel spectral behaviors. The proposed novel hierarchical scheme is developed by considering spectral change information to identify the change classes having discriminable spectral behaviors. Due to the fact that in real applications reference samples are often not available, the proposed approach is designed in an unsupervised way. Experimental results obtained on both simulated and real multitemporal hyperspectral images demonstrate the effectiveness of the proposed change-detection method.

Keywords

Change detection; hyperspectral images; multi-temporal analysis; multiple changes; hierarchical analysis; remote sensing.

I. INTRODUCTION

A comprehensive understanding of the global change is necessary for sustainable development of human society. As one of the interesting subtopics in global change study, detection of anthropogenic and natural impacts on land surface is essential for environmental monitoring. To enable a whole monitoring and evaluation of changes occurred on the ground, both long term and short term observations are required. Due to the revisit property of polar Earth Observation (EO) satellites, we can acquire remote sensing images in a given area at different times. Thus multitemporal remote sensing images are an important data source to detect the land surface changes in wide geographical areas, which is gradually reducing the need for conventional field investigations. Change Detection (CD) is the process that identifies changes occurred between two (or more) images based on the image properties [1]. The variation of image properties (e.g., pixel radiance value, texture, shape) can be related to changes on the ground at different satellite observation times. However, they may also be affected by some external factors (e.g., variation in atmospheric conditions, sensor conditions, illumination difference and seasonal effects). Automatic change-detection techniques have been widely used for remote sensing applications (e.g., ecosystem monitoring, urban area study, disaster monitoring) [2]-[4]. Nevertheless, in order to effectively perform change detection and obtain highly accurate results, it is important to devise advanced CD techniques that can automatically identify changes from multitemporal images acquired by the new generation of remote sensing satellite systems.

For decades, images acquired by multispectral (MS) medium resolution sensors have been a stable and popular data source in remote sensing change-detection applications [2],[3],[5]-[7]. With the development of sensor technology, a new generation of EO satellite sensors has been developed that can acquire images with much higher spatial and spectral resolutions. This requires the design of novel CD techniques that can address the following problems: 1) analysis of high (or very high) spatial resolution multitemporal images [1],[8],[9]; and 2) analysis of high spectral resolution (i.e., hyperspectral (HS))

multitemporal images [10],[11]. Both kinds of images contain richer change information than standard multispectral medium spatial resolution images, but also pose great challenges in the CD process. In this paper, the second problem is analyzed (refer to [1] for a detailed analysis of the first problem). We aim to define an effective approach to change detection in multitemporal hyperspectral images (CD-HS).

With the launch of HS sensors onboard of satellites (e.g., HYPERION, CHRIS, HJ-1) and the increasing use of airborne HS sensors (e.g., AVIRIS, AISA, CASI), multitemporal HS images suitable to address CD problems have been acquired. Differently from the traditional MS sensors, HS sensors can measure the solar reflected radiation in a wide wavelength spectrum (e.g., from 400 to 2500 nm) at narrow spectral intervals (e.g., 10 nm). For each pixel in HS images, a near-continuous spectral signature is obtained over the whole range of wavelengths. Therefore, CD-HS can point out small variations in the spectral signature and thus in the land surface making it possible to identify changes that are usually not detectable with MS data. However, higher spectral resolution and narrow spectral intervals directly lead to an increase of the data dimensionality, and to the presence of redundant information. This makes the change analysis more complex and challenging, especially when unsupervised methods are considered. Therefore, it is important and necessary to investigate the problem of CD-HS in order to define techniques that meet requirements of practical CD applications.

Usually, when dealing with change-detection problems in multispectral images (CD-MS), it is possible to identify abrupt land-cover changes. However, it is difficult to detect finer changes or to distinguish weaker changes associated to strong change class, due to the fact that the broadband spectral signatures do not provide enough spectral change information. The high spectral resolution of HS data allows us to address the CD problem by taking advantage of detailed spectral signatures for representing the subtle variations in complex scenarios. Let us consider a vegetated area affected by changes. On the one hand, MS images can highlight strong changes, which are class transitions that significantly affect the spectral signature (e.g., vegetation to land covers like water, built-up areas, soil). Within strong changes, other

changes may be observed that correspond to slightly different realizations of the strong change itself. In a given vegetation change class there might be more change contributions due to different factors (e.g., difference on the vegetation growth, density, water content). These kinds of change show small spectral differences with respect to those of the strong change they are associated with. Such differences are usually localized in specific parts of the spectrum. Thus it is difficult to detect them from the rough spectral representation in MS images. On the other hand, HS images can better separate different kinds of change due to the detailed representation of the spectral signatures. Moreover, if calibrated data are available, it is possible to obtain the explicit semantic meaning of the class transition ("from-to") for a change by matching each single date spectral signature with the standard reference spectra in spectral libraries. However, CD is always limited by the availability of reference samples, since both the field work and photointerpretation processes are time expensive. Therefore the design of effective unsupervised methods that are independent from ground truth data availability is highly attractive in real applications.

In this framework, we will analyze and give a definition of the CD-HS problem for a better understanding. An analysis and discussion of the concept of "change" in HS images is reported. We will concentrate on the development of effective unsupervised CD methods that: 1) address the problem of multiple-change detection; and 2) make adequate use of the detailed spectral information in HS data. Therefore we propose a novel hierarchical unsupervised CD approach that is suitable to identify different kinds of change between two HS images. The proposed approach is validated on three data sets. One is a simulated bi-temporal data set based on a HS image acquired by a commercial HS camera (Nuance FX, CRI Inc) [12]. The other two include satellite HS images acquired by Hyperion sensor (on EO-1 satellite). In order to assess the effectiveness of the proposed method for CD-HS, qualitative and quantitative assessments are conducted. From the qualitative point of view CD maps obtained with the proposed method on the three considered data sets are compared with those obtained by reference

techniques based on clustering procedures. From the quantitative point of view, performance comparison is performed by analyzing the multi-class separability among changes. Experimental results confirm the effectiveness of the proposed method.

The remainder of this paper is organized as follows. Section II gives an overview of CD techniques presented in the literatures for both MS and HS images; moreover, it addresses and formalizes the concept of CD-HS. The proposed CD method based on the hierarchical spectral change analysis is described in Section III. The HS data used for validation and the design of experiments are introduced in Section IV. Experimental results are reported and analyzed in Section V. Finally, Section VI draws the conclusion of this work.

II. CHANGE DETECTION IN HYPERSPECTRAL IMAGES

A. Overview of CD techniques for MS and HS images

For decades, CD techniques for optical images have been proposed for addressing the CD-MS problem [1]-[3], [5]-[7], [13]. These techniques can be split into two main groups: supervised and unsupervised. The supervised techniques are based on supervised classification schemes and assume that prior knowledge is available for the training of a classifier. This is the case of post-classification comparison (PCC) [14], joint-classification of multi-date images [15], compound classification [16] and classification of differential features [17]. Recently, new approaches have been proposed that assume that partial prior information is available. These approaches are based on partially unsupervised [18] or semisupervised learning [19],[20]. Such methods can be applied to both MS and HS images. However, when dealing with HS data, the attention should be devoted to define effective classification systems that: i) are suitable to the analysis of high-dimensional data and overcome the Huges phenomenon (i.e., with a fixed number of training samples, the predictive power of a classifier reduces as the dimensionality increases) [21], and ii) can effectively exploit informative features thus enhancing

change detectability. Although supervised CD methods generally outperform the unsupervised ones in detecting land-cover transitions with high accuracy, the process of collecting reference data for multitemporal images is time consuming and costly, and often unfeasible. Thus unsupervised methods are more attractive from the real application point of view.

Many methods have been developed for addressing the MS-CD problem in an unsupervised way, resulting in the definition of families of techniques aimed to: 1) binary change detection, or 2) multiple-change detection. Binary CD methods aim to only detect the presence/absence of change without giving any information about the possible separation of multiple changes. Thus all kinds of changes present on the ground are considered as a single general change class. Several methods have been proposed for binary CD [22]-[30]. From the methodological point of view, we can categorize them into thresholding-based and clustering-based techniques. In [24], the problem of binary CD was solved in an automatic way by modeling the statistical distribution of classes and incorporating spatial-context information, thus improving the previous works based on manual thresholding [22],[23]. Some techniques were designed to improve the CD performance by using optimized computation algorithms [25], ensemble learning schemes [26], data fusion approaches [27] and multi-feature strategies [28]. Clustering algorithms have been used for solving the binary CD problem as well [29],[30]. However, a more challenging goal is to distinguish among multiple changes. Some attempts based on transformation, multivariate analysis, etc., have been done to address this kind of problem in [31]-[33]. Here we recall the Compressed Change Vector Analysis (C^2VA) method recently proposed in [34], [35], which was developed based on the Polar Change Vector Analysis (CVA) approach [36]. In C^2VA the multiple-change detection problem is represented in a magnitude-direction 2-D representation generated by a lossy compression (potentially ambiguous) procedure. Despite the effectiveness of the above-mentioned methods on MS images, the problem becomes much more complex and challenging (and the efficiency of these methods is reduced) when HS images are considered. This depends on the ambiguity that is generated when compressing a

very high dimensional feature space into only two components. This is potentially critical when many changes are present.

The relatively few works present in the literature on this topic are based on: 1) transformation methods [37]-[40]; 2) spectrum analysis methods [41]-[43], and 3) other techniques [44]-[50]. Covariance equalization and cross covariance (chronochrome) are two commonly used linear transformation methods [37],[38]. They identify changes in the transformed space by subtracting feature vectors. Another class of transform-based methods represents the images in a new feature space, where the change information is concentrated into fewer components, thus reducing the high dimensionality of data and focusing on the components that are related to the specific changes of interest. Multivariate Alteration Detection (MAD) technique, which is based on the Canonical Correlation Analysis (CCA), was first introduced in [10] to solve unsupervised vegetation CD problems by using multitemporal HS images. Then it was extended to an iterative reweighted procedure (IR-MAD) in [39]. Other attempts involving Independent Component Analysis (ICA), and Temporal-PCA (TPCA) can be found in [11], [40]. After a given transformation, one (or several) component(s) can be selected for change identification. The spectrum analysis based CD method takes advantage of the detailed spectral signature in HS images. Both the distance and similarity measurements can be used to detect the difference between the considered pixel spectral signatures at two times (e.g., Spectral Angle Measure (SAM), Spectral Information Divergence (SID) and Spectral Correlation Measure (SCM) [41]-[43]). Other works have been developed to explore the problem from different perspectives: linear unmixing techniques [44]; change vector analysis after radiometric normalization [45]; model-based methods by formulating the CD as a statistical hypothesis test [46]; CD based on tensor-factorization and PCA [47]. Moreover, there are some other works focusing on the external factors that affect the CD performance, which include limiting image parallax errors [48], studying vegetation and illumination variation [49], and addressing diurnal and seasonal variations [50]. These factors may introduce errors and thus

decrease the detection accuracy, and should be limited as much as possible in real applications.

B. Challenges for change detection on hyperspectral images

HS sensors gather near-continuous spectra recording fine spectral details of the land covers or of specific targets composition. Due to the properties of HS images, the problem of CD-HS is much more challenging than that of CD-MS. The main problems associated with HS data are:

1) *High dimensionality*. It involves challenges in data handling, including storage volume and computing bottle necks, which are actually common problems for all HS data processing tasks (i.e., classification, change detection, target recognition). For CD, the main difficulty is to effectively extract changes from a high dimensionality feature space. If methods developed for MS images, like CVA or C^2VA [1], [34]-[35] are applied to a large set of spectral channels, they may fail to give a proper change representation.

2) *Information redundancy*. Continuous spectral coverage with many narrow bands does not necessarily mean higher information. Indeed, the spectral information of most of these adjacent bands results in a non-negligible redundancy. Moreover, a reduction of the signal-to-noise ratio (SNR) of the spectral signal is obtained when the spectral resolution increases from MS to HS data [51]. Therefore, information in a single HS band becomes more sparse and implicit, which may reduce the discriminability of a detector.

3) *Accurate data pre-processing*. HS data require an accurate pre-processing phase (e.g., radiometric correction, image co-registration), which may significantly affect the final CD accuracy.

Other problems arise from the methodological point of view. In greater detail we can observe that:

a) Most of the existing unsupervised CD methods directly compare and analyze the difference of pixel radiance values, ignoring the near-continuous spectrum information that is the peculiar property of HS data. The high-dimensionality and redundant information in HS data increase the noise level (with respect to MS images) thus making the change information more implicit and difficult to be identified: changes become more overlapped and less separable. Thus the identification of the number of changes

and their separation become a critical problem.

b) Most of CD-HS approaches present in the literature focus on either binary CD (i.e., detection between presence/absence of change) [43],[44] or the detection of specific changes (e.g., [10],[11], [39],[45],[47]). There is no method that addresses the challenging problem of detecting all possible kinds of change simultaneously (which can be very important especially when unexpected changes occur on the ground). Moreover, some methods still rely solely on change magnitude information [10],[11],[39], neglecting the whole spectrum information for discriminating different changes.

c) Although the transformation-based methods (e.g., MAD, IR-MAD, TPCA) allow us to detect multiple changes [10],[11],[39],[40], the application of transformation to high-dimensionality data results in a high computation cost, in a difficult interpretation of all components and in a qualitative and ambiguous description of change classes, especially for subtle changes.

d) Definition and description of the detected changes are still rough and unclear. Although the unsupervised approaches are not capable to provide the "from-to" transition information, it is necessary to define methods that are able to differentiate the detected changes related to different land-cover transitions.

e) The existing methods try to extract all change classes directly from the original data space or from a transformed feature space relying only on a single operation (e.g., transformation, differencing), which increases the difficulty of separating multiple change classes and thus affects the detection accuracy.

C. Analysis of the change concept in multitemporal HS images

The aim of this work is to propose a method that is able to identify all class transitions having discriminable spectral behaviors either globally or locally in the spectrum of multitemporal HS images. These class transitions are defined here as *change endmembers*.

In order to conduct an effective CD-HS, it is important to understand and model the concept of "change" in multitemporal HS images and its relationship with the concept of endmember. The very high spectral

resolution makes it possible to detect many differences in the spectral signatures of pixels acquired in a scene of interest. Such differences may occur at different spectral resolution levels.

Let us consider two HS images $\boldsymbol{X_1}$ and $\boldsymbol{X_2}$ with size $P \times Q$, acquired on the same geographical area at times t_1 and t_2, respectively. To analyze the behaviors of spectral differences between the two images, let us compute the HS difference image $\boldsymbol{X_D}$ by subtracting multitemporal images from each other pixel by pixel [34].

$$\boldsymbol{X_D} = \boldsymbol{X}_2 - \boldsymbol{X}_1 \tag{1}$$

Let $\boldsymbol{x_i}$ be a Spectral Change Vector (SCV) with spatial position i (i =1,…, $P \times Q$) in $\boldsymbol{X_D}$, $\boldsymbol{x_i} \in \boldsymbol{X_D}$. In such image each pixel is characterized by a SCV that shows as many elements as the spectral channels in the original HS images. Each element assumes values that depend on whether a change occurred or not for a specific wavelength, and on the kind of change. Therefore, we use SCV signatures that are related to the land-cover class transitions, to formalize the considered problem.

Generally speaking, a pixel can belong to the class of changed pixels Ω_c or the one of unchanged pixels ω_n according to the magnitude of its SCV [36]. Fig.1 (a) gives a qualitative example of the expected behavior of the magnitude of $\boldsymbol{X_D}$. Unchanged pixels show a SCV magnitude close to zero (blue mode in Fig.1.a). The SCV signatures of such pixels have all spectral components close to 0 (see the blue signature in Fig.1.b). Changed pixels show high magnitude values (red mode in Fig.1.a), and their SCV signature shows one or more components that are far from 0. It is worth noting that in the 1-D magnitude domain usually all changes contribute to a single class Ω_c, since different kinds of change cannot be separated in the magnitude domain (see Fig.1.a). A finer analysis of SCV behaviors points out that Ω_c may include contributions from several change classes (see red and green signatures associated in Fig.1.b) depending on how the specific kind of change impacted on the spectral signature. SCVs can be preliminary separated into *major changes*. Major changes mainly depend on the land-cover class

transitions and have a large spectral difference with respect to no-change class and among each other. Usually, major changes can be easily and directly identified as they significantly affect a large portion of the spectrum of HS images. In many cases they can be also detected from MS images. As shown in Fig.1 (c), each major change (i.e., ω_{C_1} and ω_{C_2}) produces statistically significant different spectra compared with each other and with the class of unchanged pixels. Within each major change, depending on the data, it is possible to detect other clusters of pixels having significant statistical differences in some parts of the spectrum. Such clusters are defined here as s*ubtle changes*. Subtle changes have SCVs similar to a major change, but differ from it in small portions of the spectrum. In Fig.1 (c), subtle changes $\omega_{C_{1\text{-}1}}$ (in purple) and $\omega_{C_{1\text{-}2}}$ (in orange) belong to the same major change ω_{C_1} (in red), whereas $\omega_{C_{2\text{-}1}}$ (in magenta) and $\omega_{C_{2\text{-}2}}$ (in sea green) belong to ω_{C_2} (in green). In other words subtle changes shows SCVs statistically different each other in some component of the spectrum, but quite similar to those of the associated major change. Subtle changes can be therefore detected only if a fine sampling of the spectral signature is available as it happens in HS images. If the sampling is poor as in the case of MS images, they cannot be detected.

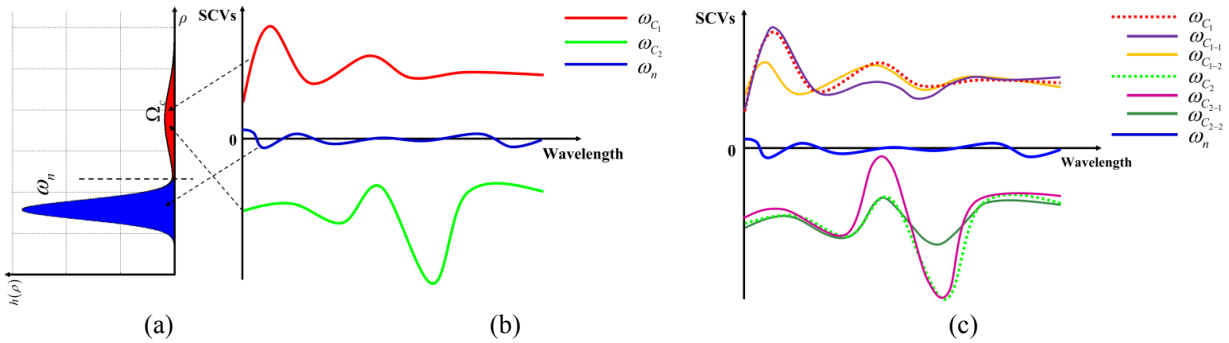

(a) (b) (c)

Fig.1 Qualitative illustration of (a) the statistical distribution of the magnitude of SCVs ($h(\rho)$); the sample spectra on SCVs of major and subtle change classes that defined in multitemporal HS images: (b) major changes; (c) subtle changes (solid line) within the given major changes (dotted line).

According to the above discussion $\Omega_c = \{\omega_{C_1}, \omega_{C_2}, ...\}$ is the set of major changes, i.e., changes that affect a large part of the spectrum and that have statistical properties significantly different from each other.

Each major change may include subtle changes (i.e., $\omega_{C_1} = \{\omega_{C_{1\text{-}1}}, \omega_{C_{1\text{-}2}}, ...\}$ and $\omega_{C_2} = \{\omega_{C_{2\text{-}1}}, \omega_{C_{2\text{-}2}}, ...\}$) whereas others may not (i.e., $\omega_{C_3} = \varnothing$). By iterating the process it is possible to state that each subtle change can be further split until it is not possible to detect statistical inhomogeneity. Each major or subtle change that cannot be split anymore is defined as *change endmember*[1]. Accordingly, all pixels associated with a specific change endmember have the same (or very similar) spectral behaviors in the SCV domain and thus can be clustered into the same group. Let $\Omega_e = \{e_1, e_2, \ldots, e_E\}$ be the set of E possible change endmembers. Let e_n be the endmember associated to no-changed pixels. Thus the problem that we need to address is related to the identification and separation of change endmembers from each other and from unchanged pixels. We assume that the considered images are all radiometric corrected, thus change endmembers are only related to the application and the end-user. Note that the external factors (e.g., illumination conditions, seasonal effects) might have impacts on the detected change endmembers (causing differences) but will not be identified as one of them due to its low change magnitude.

III. PROPOSED HIERARCHICAL APPROACH TO THE DETECTION OF MULTIPLE CHANGES IN HYPERSPECTRAL IMAGES

Based on the discussion, definitions and assumptions presented in the previous section, we propose a novel hierarchical CD method for detecting changes in HS images and separating them into different change endmembers. The proposed method mainly consists of three steps: a) pseudo-binary change detection to initialize the process and extract general changes; b) change endmember detection based on hierarchical spectral change analysis; and c) generation of the CD map by merging endmember clusters. The block scheme of the proposed approach is illustrated in Fig.2.

[1] Note that the definition of change endmember is in concept different from the definition of endmembers in spectral unmixing. In the latter case, endmembers are the spectral signatures of pure classes that result combined in mixed pixels due to the limited spatial resolution of the acquisition sensor.

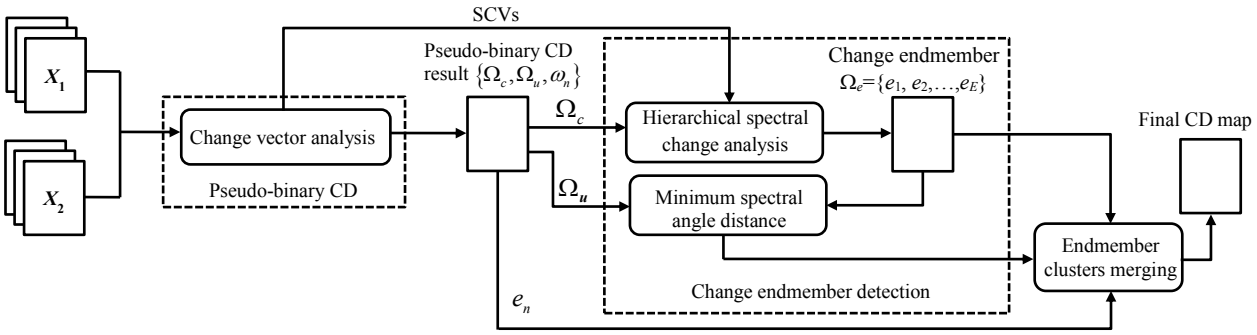

Fig.2 Block scheme of the proposed change-detection approach to multitemporal hyperspectral images.

A. Pseudo-binary change detection

This step is based on the analysis of the magnitude of SCVs according to traditional binary CD techniques. However it is referred as pseudo-binary because the output has three classes. After separating the change (Ω_c) and no-change (ω_n) classes (thus no-change endmember e_n is straightforward), an uncertainty buffer class (Ω_u) is defined. The class of changes (Ω_c) is used to initialize the root node of a tree structure for change representation.

From $\boldsymbol{X_D}$ the magnitude and the direction of SCVs can be extracted. In the first step of the proposed method we are only interested in distinguishing Ω_c from ω_n. Thus only the magnitude ρ is considered:

$$\rho = \sqrt{\sum_{b=1}^{B} (\boldsymbol{X}_D^b)^2} \tag{2}$$

where B denotes the number of spectral channels of the HS images (i.e., the dimensionality of SCVs), and $\boldsymbol{X}_D^b$ is the b-th spectral difference in $\boldsymbol{X_D}$. Thus the whole B-D change information is compressed into a 1-D feature. The rationale behind this choice is: 1) to simplify and avoid any feature selection procedure; 2) to exploit the contribution of all portions of the spectrum. If noisy bands are detected in the pre-processing (e.g., due to atmosphere absorption) they can be neglected.

Changed and unchanged pixels are separated into two groups according to a threshold value T_ρ computed on the magnitude variable. The Bayesian decision theory is applied to find this threshold [24].

The Expectation Maximization (EM) algorithm is used for estimating the class statistical parameters (i.e., the class prior probabilities, the mean values and variances) in an unsupervised way [24], [52]. Note that change and no-change classes are assumed to be Gaussian distributed, and multiple changes are approximated as one single change class (Ω_c) in the magnitude domain to focus only on the general change information. This approach has been widely used in binary CD with MS images and demonstrated to be a good approximation in HS images [1], [34]-[36]. The approximation is acceptable as this is only a preliminary step.

In order to reduce the effect of possible thresholding errors and obtain conservative results that do not propagate significant errors in the next steps, a margin δ is set on the threshold computed on the histogram $h(\rho)$ of the magnitude ρ (see Fig.3) and three classes are defined. The three classes are: 1) *class of uncertain pixels* (Ω_u), on which it is not possible to take a reliable decision at this level of the processing. These pixels will be analyzed and reclassified according to the generated endmembers; 2) *class of changed pixels* (Ω_c), which includes pixels having a high probability to be changed, but without any information on their kind. The problem of the multiple changes identification will be addressed in the next step by the proposed hierarchical spectral change analysis method; 3) *class of no-changed pixels* (ω_n), which only contains pixels having a high probability to be unchanged. These pixels are treated as a pure no-change class endmember due to their low magnitude. Thus for a given SCV $\boldsymbol{x_i}$ in $\boldsymbol{X_D}$, a label is assigned according to the following rule:

$$\boldsymbol{x_i} \in \begin{cases} \Omega_c, & \text{if } \rho_i \geq T_\rho \\ \Omega_u, & \text{if } T_\rho - \delta \leq \rho_i < T_\rho \\ \omega_n, & \text{if } \rho_i < T_\rho - \delta \end{cases} \tag{3}$$

where ρ_i is the SCV magnitude of the considered $\boldsymbol{x_i}$. Fig.3 illustrates the flowchart of the pseudo-binary CD step.

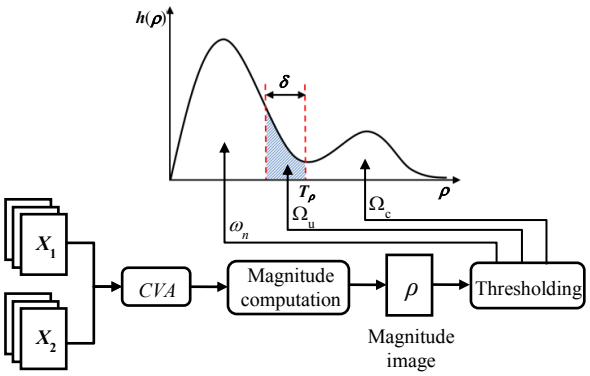

Fig.3 Block scheme of the pseudo-binary change-detection step used for initializing the tree structure.

B. Endmember detection based on hierarchical spectral change vector analysis (HSCVA)

Let us focus on the classes of changed (i.e., Ω_c) and uncertain (i.e., Ω_u) pixels obtained in the previous step for identifying the change endmembers. The problem can be addressed by using clustering methods to automatically find the different change classes. However, the problem of multiple-class separation in HS images is much more difficult than in MS images. This is due to the following issues: 1) the high spectral resolution makes the spectrum more sensitive to changes, thus a high number of changes might be detected; and 2) subtle changes within major changes are always difficult to be identified directly from Ω_c. These problems decrease the detectability of all the hierarchy of changes directly from the data in one shot, and limit the effectiveness of clustering methods.

To overcome the mentioned problems, we propose a solution based on the idea of decomposing the original complex problem into sub-problems by a *Hierarchical Spectral Change Vector Analysis* (HSCVA) (see Fig.4 for a qualitative example of hierarchy). The hierarchical structure is modeled by a tree of changes defined to drive the analysis. Let L_d be a generic level in the tree structure with d = 0, 1,…, D-1. The depth of the tree is D (e.g., D=4 in Fig.4). The main idea is to start from the root node in the top level (i.e., L_0 that represents the general change class Ω_c identified in the pseudo-binary CD step) and gradually separate different kinds of change into child nodes by selectively exploiting the spectral

information. At the first level (i.e., L_1) of the tree the priority is given to identify the major changes that according to the definition of Section.II.C have significant spectral difference from each other. Within each child node, subtle changes (if any) are detected and separated. This process is iterated until all change endmembers (i.e., leaves of the tree) are found.

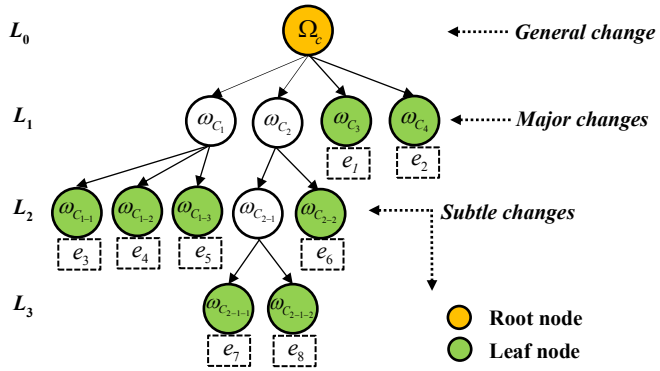

Fig.4 Example of the proposed hierarchical tree for the detection of change endmembers with tree depth *D*=4 and 8 identified leaves.

Let us consider the root node that contains all the changed pixels without any distinction about their kind. To model the spectral homogeneity of Ω_c, a similarity measure based on the Spectral Angle Distance (SAD) [53] is used. The SAD ϑ is computed between each $\boldsymbol{x_i}$ in Ω_c, and a reference spectral signature $\boldsymbol{S}_{\Omega_c}$ calculated as the average of all the $\boldsymbol{x_i}$ in Ω_c, i.e.,

$$\vartheta(\boldsymbol{x}_i, \boldsymbol{S}_{\Omega_c}) = \arccos\left(\frac{\sum_{b=1}^{B} \boldsymbol{x}_i^b \boldsymbol{S}_{\Omega_c}^b}{\sqrt{\sum_{b=1}^{B} \left(\boldsymbol{x}_i^b\right)^2} \sqrt{\sum_{b=1}^{B} (\boldsymbol{S}_{\Omega_c}^b)^2}} \right), \quad \boldsymbol{x}_i \in \Omega_c \tag{4}$$

$\boldsymbol{x}_i^b$ and $\boldsymbol{S}_{\Omega_c}^b$ are the b-th component in $\boldsymbol{x_i}$ and $\boldsymbol{S}_{\Omega_c}$, respectively. For each $\boldsymbol{x_i}$, the smaller $\vartheta(\boldsymbol{x}_i, \boldsymbol{S}_{\Omega_c})$, the higher the similarity with the reference spectrum and vice versa. For a pure change endmember we expect that all SCVs have very similar spectral behaviors, thus resulting in a small standard deviation of the similarity measure. Thus to verify the homogeneity of Ω_c we compare the standard deviation value

$\sigma_{\vartheta_{\Omega_c}}$ of $\vartheta(\boldsymbol{x}_i, \boldsymbol{S}_{\Omega_c})$ with a threshold value T_σ. If $\sigma_{\vartheta_{\Omega_c}}$ is smaller than T_σ, the change class is considered as being homogeneous and a change endmember is detected. Accordingly, the process is in convergence and the tree only has a single node. Otherwise the change class is considered as being inhomogeneous and likely to contain more than one kind of change. Therefore the hierarchical decomposition starts.

To distinguish major changes in Ω_c Principal Component Analysis (PCA) and clustering algorithm are used. However, any other transformation technique can be considered. Note that PCA is applied only to the $\boldsymbol{x_i}$ belonging to Ω_c. In this way we optimize the representation of the changes. Then the clustering algorithm is applied to the subset of transformed Principal Components (PCs) that includes more than 95% of change information to reject the noise and redundant information. This choice also reduces the computational complexity. Let $\boldsymbol{P}$ be the image with selected M ($M < B$) PCs and let $\boldsymbol{P_i}$ be the vector characterizing spatial position i (i =1,…, $P \times Q$) in $\boldsymbol{P}$, $\boldsymbol{P_i} \in \boldsymbol{P}$. An effective clustering technique should be used to correctly identify the major change classes inside Ω_c. The following issues need to be addressed: 1) identification of the number of major changes; 2) definition of a strategy for modeling and clustering the change information.

In order to address the above two issues, the adaptive *x*-means algorithm is used to automatically find an optimal number of major changes and generate reliable clustering results in an unsupervised framework [54],[55]. Differently from the popular *k*-means method, *x*-means adaptively searches on a range of *k* values and finds the best clustering model according to the Bayesian Information Criterion (BIC) [54]. The BIC identifies an adequate tradeoff between simplicity of the model (number of parameters) and quality of fit. It analyzes the maximum likelihood-based models of a given data distribution. We adopt the algorithm proposed in [55], which is an expansion of the original *x*-means, and modified it in order to satisfy our requirements. A given range $U = [k_0, k_0+t]$ is first defined to initialize the *x*-means. This is the only input parameter to the algorithm. k_0 denotes the lower bound for the number of major changes k,

and t is a constant value to control the upper bound. Then M-dimensional PCs of Ω_c are given as input to the x-means clustering and the method is initialized by applying conventional k-means with $k = k_0$. We assume that all kinds of change approximately follow the Gaussian distribution. The BIC value of each generated cluster is then compared with the joint BIC value of its split into two clusters, and the clusters associated with the smaller value are selected (the smaller BIC value the better fitting is) [54]. An additional merging operation is applied if necessary to ensure that the final output number of clusters is within the defined range U [55]. After applying the x-means clustering, the final output includes: 1) the optimal number k of major changes; 2) the detected major changes in Ω_c (i.e., the level L_1 of the hierarchical tree structure). Note that BIC is just one of the choices for the optimal model selection. However, it is a reliable criterion especially for normal distributions. Other test criteria, such as Akaike Information Criterion (AIC) and Minimum Description Length (MDL) may also be used [56], [57].

To define a reliable range U for the clustering process, the initial number of classes should be identified, which is the lower bound k_0 ($k_0 \geq 2$) in the x-means. k_0 should be small enough to include the minimum number of change classes that can be directly recognized. To perform a reliable choice of this parameter, we applied a method based on the analysis of the compressed change direction representation proposed in [34]. Instead of directly computing the angular distance in the original feature space, we computed it on the selected M-dimensional PCs of Ω_c as follows:

$$\varphi(\boldsymbol{P_i}) = \arccos\left(\frac{1}{\sqrt{M}} \left(\sum_{m=1}^{M} P_i^m \Big/ \sqrt{\sum_{m=1}^{M} (P_i^m)^2} \right) \right) \tag{5}$$

where $\varphi(\boldsymbol{P_i})$ is the compressed change direction of $\boldsymbol{P_i}$, and P_i^m is the m-th component of vector $\boldsymbol{P_i}$. In this way we emphasize in the direction variable only the possible changes associated with Ω_c. The first PCs can properly model the changes that we are looking for. Thus the modes of the obtained distribution on the compressed change direction $\varphi(\boldsymbol{P_i})$ can be recognized as the initial number k_0 of major changes

existing in Ω_c (see Fig.5). The upper bound of the range U is defined by adding a small integer value t to k_0. t is in the order of few units and takes into account the intrinsic uncertainty of defining k_0 by analyzing $\varphi(\boldsymbol{P_i})$.

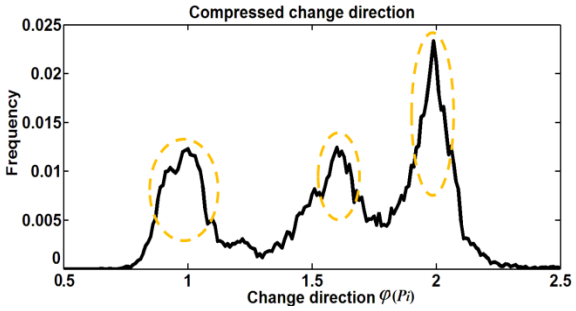

Fig.5 Example of definition of the initial cluster number (k_0) based on analyzing of the compressed change direction.

Once the major change classes in Ω_c have been recognized and separated by using the adopted clustering algorithm, the root node splits into different child nodes at L_1 in the tree. Each node corresponds to one major change class (i.e., $\omega_{C_1}, \omega_{C_2}, \ldots$). For each major change $\omega_{C_1}, \omega_{C_2}, \ldots$ the spectral homogeneity of SCVs is tested according to (4). As an example let us consider the first child node associated to class ω_{C_1}. The SAD of ω_{C_1} is computed as $\vartheta(\boldsymbol{x_i}, \boldsymbol{S}_{\omega_{C_1}})$ for each $\boldsymbol{x_i} \in \omega_{C_1}$. If for a given node convergence is not reached (e.g., in our example it means that the standard deviation of $\vartheta(\boldsymbol{x_i}, \boldsymbol{S}_{\omega_{C_1}})$ is larger than a given threshold) then all the above operations (i.e., PCA, x-means, stop criterion evaluation) are iterated by considering only the SCVs of pixels $\boldsymbol{x_i}$ in the considered node (e.g., ω_{C_1} in our example). Once all the nodes at L_1 are processed, the algorithm moves to the next level. The hierarchical decomposition is applied to each node in every level of the tree until the convergence is reached for all of them (see Fig.6). This happens when all the nodes satisfy the homogeneous condition in (4). The last node of each branch is a leaf node and corresponds to one change endmember in $\Omega_e=\{e_1, e_2, \ldots, e_E\}$. Note that at convergence change endmembers can appear at different levels of the tree. The block scheme of this step is shown in

Fig.6.

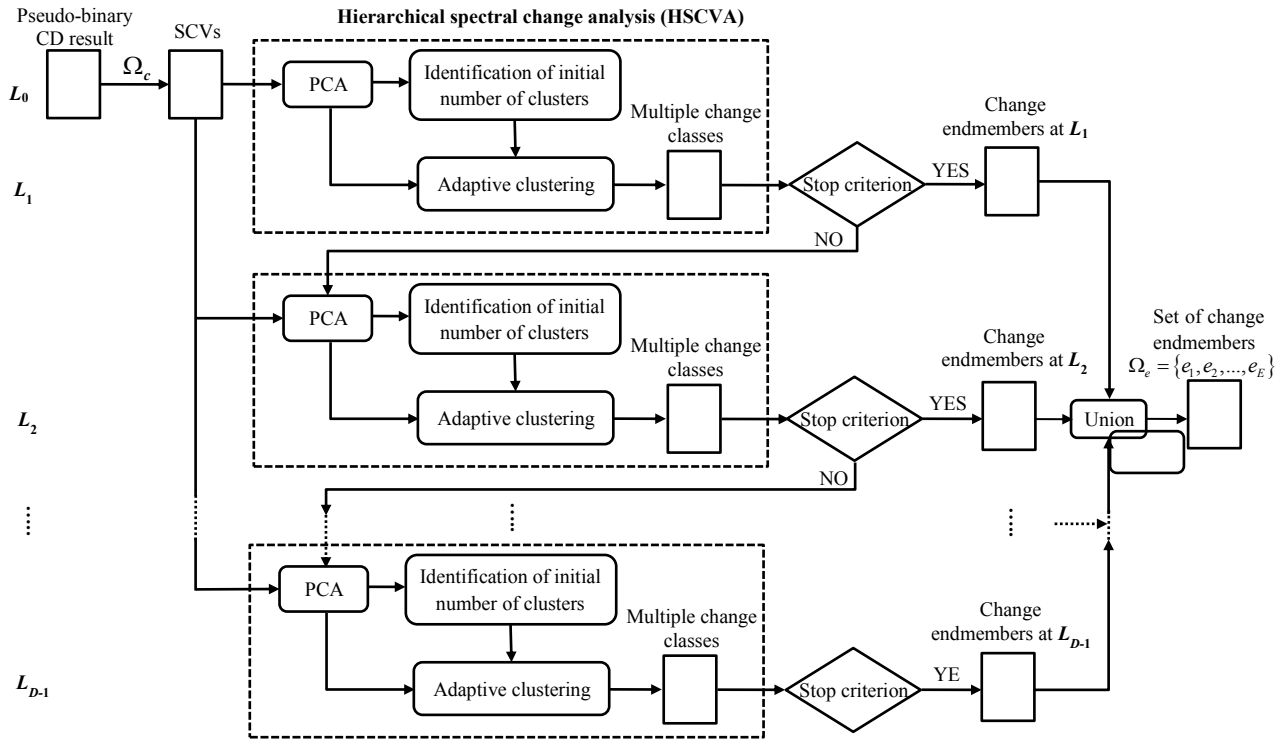

Fig.6 Block scheme of the HSCVA step in the proposed change-detection approach.

C. Generation of the change-detection map by endmember clusters merging

After identifying E change endmembers $\Omega_e = \{e_1, e_2, \ldots, e_E\}$, the pixels in the uncertain class Ω_u derived in the first step of pseudo-binary CD are considered. These pixels are assigned to one of the change endmembers or to the no-change class on the basis of spectral similarity. SAD (see (4)) is computed between the SCV $\boldsymbol{x_i}$ ($\boldsymbol{x_i} \in \Omega_u$) and the reference spectra $\boldsymbol{S}_{e_j}$ (i.e., the average spectrum of each detected change endmember in Ω_e and of the no-change endmember e_n). Then $\boldsymbol{x_i}$ is assigned to the class with the minimum distance value, i.e.,

$$\boldsymbol{x_i} \in \underset{e_j \in \{\Omega_e, e_n\}}{\arg\min} \left\{ \vartheta(\boldsymbol{x_i}, \boldsymbol{S}_{e_j}) \right\} \tag{6}$$

where $\vartheta(\boldsymbol{x_i}, \boldsymbol{S}_{e_j})$ denotes the SAD distance between $\boldsymbol{x_i}$ ($\boldsymbol{x_i} \in \Omega_u$) and a given reference spectrum $\boldsymbol{S}_{e_j}$.

The final CD map is generated by merging the results obtained in the three sets of changed, uncertain and unchanged pixels (see in Fig.2).

IV. DATA SET DESCRIPTION AND DESIGN OF EXPERIMENTS

A. Description of Data sets

1) *Simulated hyperspectral data set*: the first data set is taken from a real-world database of HS images presented in [58], which includes images acquired by a commercial HS camera (Nuance FX, CRI Inc.) [12]. With an integrated liquid crystal tunable filter, the camera acquires HS images by sequentially tuning the filter through a series of 31 narrow wavelength bands. The bandwidth is approximately 10nm in a wavelength range from 420nm to 720nm, covering mainly the visible spectrum region. The selected image is an outdoor scene in the Harvard University with a size of 1392×1040 pixels (see Fig.7.a). In order to simulate the change targets and build the synthetic dataset, eight tiles were extracted from the original image ($\boldsymbol{X_1}$) over all the spectral bands (see colored rectangles in Fig.7.a). They correspond either to different materials of the wall in the scene or to the same material, but under different illumination conditions. Tiles were inserted into disjoint areas on a copy of the original image to generate a simulated image ($\boldsymbol{X_2}$) showing changes associated either to the material transitions or to the same material transitions but affected by different illumination conditions. By doing this, we simulated the subtle changes and increased the complexity of the considered problem. The same simulation setup was conducted three times by varying the position of tiles, thus generating three simulated multitemporal datasets. Each one is composed of $\boldsymbol{X_1}$ and one among the three simulated $\boldsymbol{X_2}$. Fig.7 (b) shows one of the simulated images, and Fig.7 (c) presents the corresponding change reference map, which includes 10 change endmembers. The performance indices for this data will be presented as the average values over the three simulated data sets.

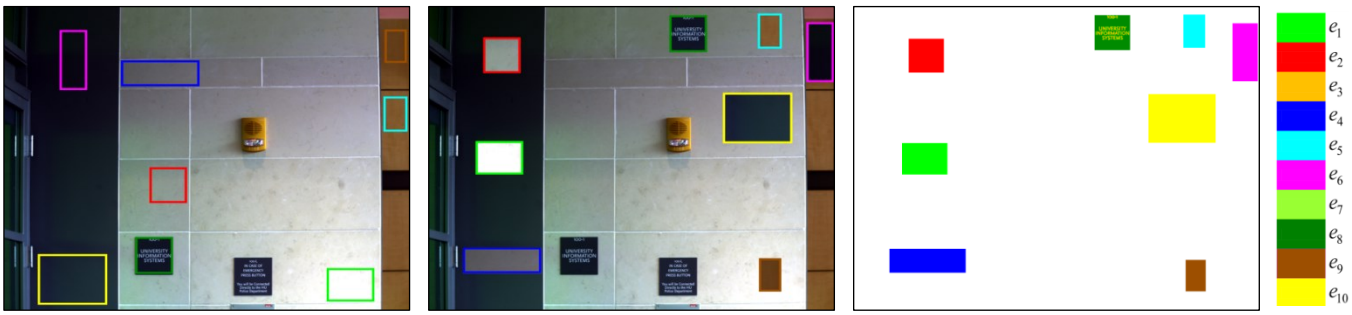

(a) (b) (c)

Fig.7 False color composite (R: 710nm; G: 620nm; B: 510nm) of (a) the HS image acquired by the Nuance FX HS camera (X_1); (b) one of the simulated image (X_2) with changes; (c) Reference map (10 changes in different colors, no-change class in white color).

2) *Hyperion satellite images of an irrigated agricultural area*: The second data set is made of a pair of real bi-temporal HS remote sensing images having a size of 211×396 pixels. These images were acquired by the Hyperion sensor mounted onboard the Earth Observing-1 (EO-1) satellite on May 1st, 2004 ($\boldsymbol{X_1}$) and May 8th, 2007 ($\boldsymbol{X_2}$). The images were downloaded from the U.S. Geological Survey (USGS) website [59] using the EarthExplorer GUI. Fig.8 (a) and (b) shows a false color composite of the two images. The study area covers an irrigated agricultural land of Hermiston city in Umatilla County, Oregon, United States. Land-cover changes include the transitions among the crops, soil, water and other land-cover types. The changes occurred in the crop land are mainly due to the vegetation water content that affected the irrigation condition in the field (see the circles on the image, which correspond to the radius of the irrigation system), and to the difference of the crop growth situation. The original Hyperion images contain 242 spectral bands, ranging from 350nm to 2580nm (i.e., visible, near infrared, short-wave infrared), with a spectral resolution of 10nm and a spatial resolution of 30m. Pre-processing was applied to the images, including bad stripes repairing, atmospheric corrections, and image co-registration with a residual error of 0.5 pixels. Radiometric correction was conducted to mitigate differences in illumination conditions and their impact on the CD step, thus reducing changes that are mainly irrelevant to the application and the end-users. In addition, we removed the uncalibrated bands

(according to the prior knowledge on the Hyperion sensor), the overlapped redundant bands and the noisiest bands due to low SNR values [60]. It should be noted that even if we removed the noisiest bands and uncalibrated bands, the selected channels include both clean and partially noisy bands, which still maintain the complexity of the data. Finally, 159 pre-processed bands (i.e., 8-57, 82-119, 131-164, 182-184, 187-220) were selected for performing the CD task. However, no ground truth samples are available for this data set. Thus the validation of results is done mainly in a qualitative way. Fig.8 (c) represents a false color composite of spectral channels in $\boldsymbol{X_D}$. Different colors indicate possible kinds of change classes, whereas gray areas represent the unchanged pixels. The same change class can be described differently in different wavelengths (e.g., see Fig.8 (d) and (e) where the same kind of change is highlighted in orange and green circles and has different behaviors in bands 30 and 40 of $\boldsymbol{X_D}$). Accordingly the two examples given in Fig.8 do not fully describe the complexity of the problem.

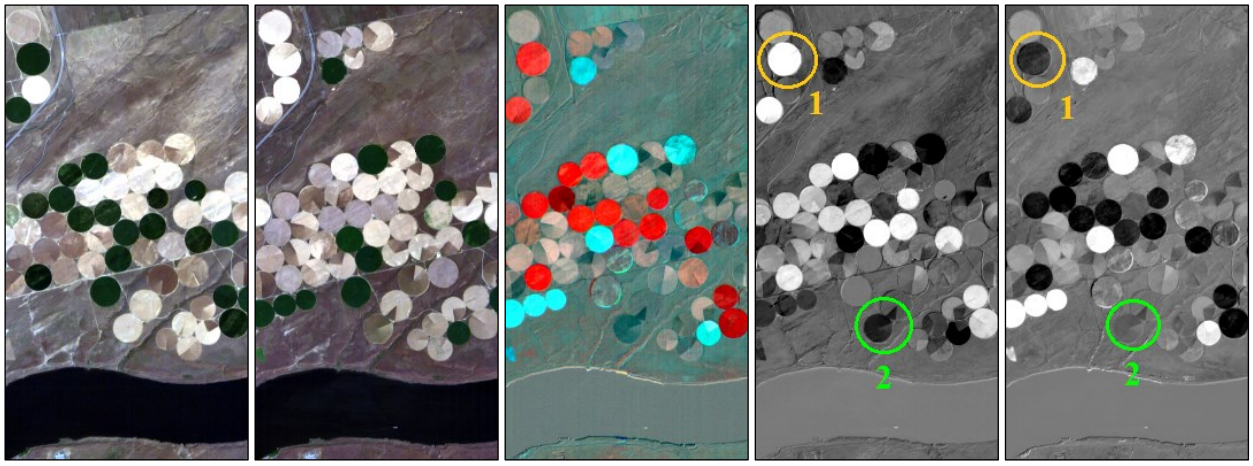

(a) (b) (c) (d) (e)

Fig.8 Hyperion images acquired on an irrigated agricultural area. False color composite (R: 650.67nm, G: 548.92nm, B: 447.17nm) of the original images acquired in (a) 2004 (X_1) and (b) 2007 (X_2); (c) composite three SCVs channels (R: 1729.70nm, G: 1023.40nm, B: 752.43nm); single SCVs channel of (d) band 30 (650.67nm) and (e) band 40 (752.43nm).

3) *Hyperion images of wetland agricultural area*: Another pair of bi-temporal Hyperion HS images with a size of 252×526 pixels, acquired on May 3, 2006 ($\boldsymbol{X_1}$) and April 23, 2007 ($\boldsymbol{X_2}$) in a wetland agricultural area in Yancheng, Jiangsu province, China, was used in the experiments. These images were also

downloaded from U.S. Geological Survey (USGS) website [59]. After applying the same pre-processing used for the previous data set, 132 bands were selected: 13-53, 83-96, 101-118, 135-164, 188-199 and 202-218. Also for this dataset we do not have any available ground truth. False color composite images of the bi-temporal data are shown in Fig.9 (a) and (b). In this scenario, the land-cover classes mainly include the agricultural cropland, seafood farm ponds, and offshore shoals vegetation (e.g., spartina alterniflora, suaeda and reed). During the study period, the actual land-cover changes included transitions among vegetation (most were in the crop field), water area, seafood farm ponds and some buildings. Fig.9 (c) shows a false color composite image of $\boldsymbol{X_D}$, and Fig.9 (d) and (e) present some selected channels of $\boldsymbol{X_D}$. Similarly as before, the false color composition does not fully describe the complex CD problem. However, it gives an idea about where the changes occurred.

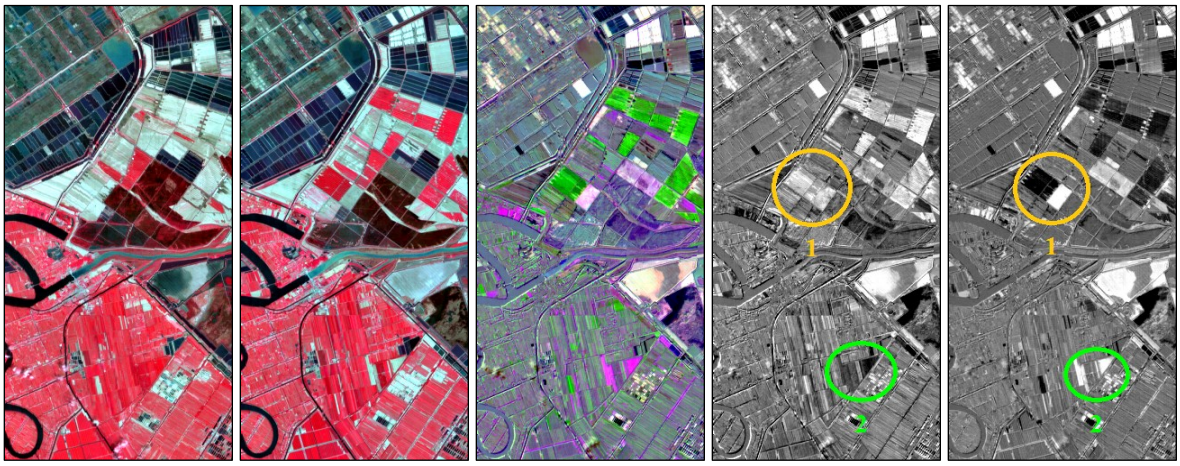

(a) (b) (c) (d) (e)

Fig.9 Hyperion images acquired on a wetland area in China. False color composite (R: 752.43nm, G: 650.67nm, B: 548.92nm) of the original images acquired in (a) 2006 (X_1) and (b) 2007 (X_2); (c) composite of SCVs channels (RGB: 1729.70nm, 752.43nm, 650.67nm); selected SCVs channels: (d) band 52 (874.52nm) and (e) band 158 (1729.70nm).

B. Design of Experiments

The proposed CD approach has been applied to the three HS data sets. For the synthetic bi-temporal HS images, the same procedure was conducted on three simulated data sets (see Section.III.A). In this case, the first step of pseudo-binary CD was neglected as the general change class Ω_c is explicitly defined by the change simulation step. Thus we directly focused on the pixels in Ω_c and tried to identify different

change endmembers inside it. Performance is assessed quantitatively on the three reference maps. The final performance indices are given as the average accuracy over the three simulated datasets. For the two Hyperion HS remote sensing data sets, the proposed method was applied starting from the pseudo-binary CD step and the three clusters (Ω_c, Ω_u and ω_n) where generated. The value δ was set such that the Ω_u class includes 25% of the pixels in ω_n. After obtaining the general change class Ω_c, T_σ was set to drive the decomposition of the root node and to build the hierarchical tree for change endmember detection. T_σ is a user dependent parameter and controls the level of spectral homogeneity of the detected change endmembers. The smaller the threshold value T_σ, the higher the homogeneity level is and thus the number of change endmembers, and viceversa. In practical applications, the threshold should be selected taking into account the desired sensitivity to subtle changes. In our experiments trials were carried out with different values of T_σ, achieving different trade-offs in terms of endmember homogeneity.

After the initialization of Ω_c (i.e., root node of the tree), the identification of multiple change endmembers was done by using the proposed HSCVA step. The initial number of k_0 was defined based on the compressed change direction method described in Section III, and t was set equal to 3 to define the upper bound of U. The final CD map was obtained when all change endmembers were generated and the pixels in Ω_u were assigned to one of them or to the unchanged endmember. The results obtained by the proposed method were compared with the ones obtained by the popular unsupervised k-means and fuzzy C-means (FCM) clustering methods. The two reference methods were applied to the subset of PCs selected by the proposed method for the root node, i.e., the ones that contain most of the information for Ω_c. The class number k of k-means and FCM was fixed on the basis of the proposed method outcome. In this way, we give clear advantage to the reference techniques that have not the intrinsic capability to estimate the number of expected change endmembers. This choice implicitly penalizes the proposed

method. To reduce the uncertainty due to the random initialization in the reference methods, we ran them 200 times. The final accuracy was calculated as the average over 200 trials.

To evaluate the CD results both quantitative and qualitative assessments were carried out for each of the three considered datasets. For the synthetic data set, the quantitative assessment was based on the CD accuracy (i.e., endmember accuracy and kappa accuracy) and error indices obtained according to the reference maps. In addition, the average endmember distance has been computed to assess the average endmember separability. To this end, pair-wise Bhattacharyya distance was computed among all the pairs of change endmembers. For two generic detected change endmembers e_α and e_β ($\alpha, \beta \in [1,E]$ and $\alpha \neq \beta$), the Bhattacharyya distance $B_{\alpha,\beta}$ is calculated as follows:

$$B_{\alpha,\beta} = \frac{1}{8}(\boldsymbol{\mu}_\alpha - \boldsymbol{\mu}_\beta)^T \left\{ \frac{\boldsymbol{\Gamma}_\alpha + \boldsymbol{\Gamma}_\beta}{2} \right\}^{-1} (\boldsymbol{\mu}_\alpha - \boldsymbol{\mu}_\beta) + \frac{1}{2} \ln \left\{ \frac{\left| \left(\boldsymbol{\Gamma}_\alpha + \boldsymbol{\Gamma}_\beta \right) / 2 \right|}{\left| \boldsymbol{\Gamma}_\alpha \right|^{1/2} \left| \boldsymbol{\Gamma}_\beta \right|^{1/2}} \right\} \tag{7}$$

where $\boldsymbol{\mu}_\alpha$ and $\boldsymbol{\mu}_\beta$ denote the mean vectors, $\boldsymbol{\Gamma}_\alpha$ and $\boldsymbol{\Gamma}_\beta$ represent the covariance matrices of change endmembers α and β, respectively. The higher distance the better the class separability, and viceversa. The average pairwise Bhattacharyya distance computed on all pairs of change endmembers gives indication of the overall class separability. In the following we will refer to it as multi-class Bhattacharyya distance.

The CD results were also analyzed qualitatively by comparing: 1) the obtained CD maps; 2) the 2-D scatterplots of change endmembers in the feature space (i.e., the first PC versus the second PC on Ω_c); 3) the spectral signatures of all the detected change endmembers in $\boldsymbol{X_D}$ with the ones obtained with reference techniques.

V. EXPERIMENTAL RESULTS AND DISCUSSION

A. Simulated hyperspectral data set

For the simulated data, experimental results were obtained by fixing the value of T_σ to 0.05 for all the

three image pairs. The average kappa accuracy (κ) and the average multi-class Bhattacharyya distance obtained by the three considered methods are shown in TABLE I. As one can see, the proposed method obtained both the highest kappa accuracy and the highest average Bhattacharyya distance.

TABLE I
AVERAGE KAPPA ACCURACY AND MULTI-CLASS BHATTACHARYYA DISTANCE OBTAINED BY THE THREE CONSIDERED METHODS ON THE SIMULATED DATA SETS.

Method	Average κ	Average multi-class *Bhattacharyya* distance
PCA *k*-means	0.9772±0.0007	5.28
PCA FCM	0.9002±0.0012	5.03
Proposed method	0.9930±0.0009	5.91

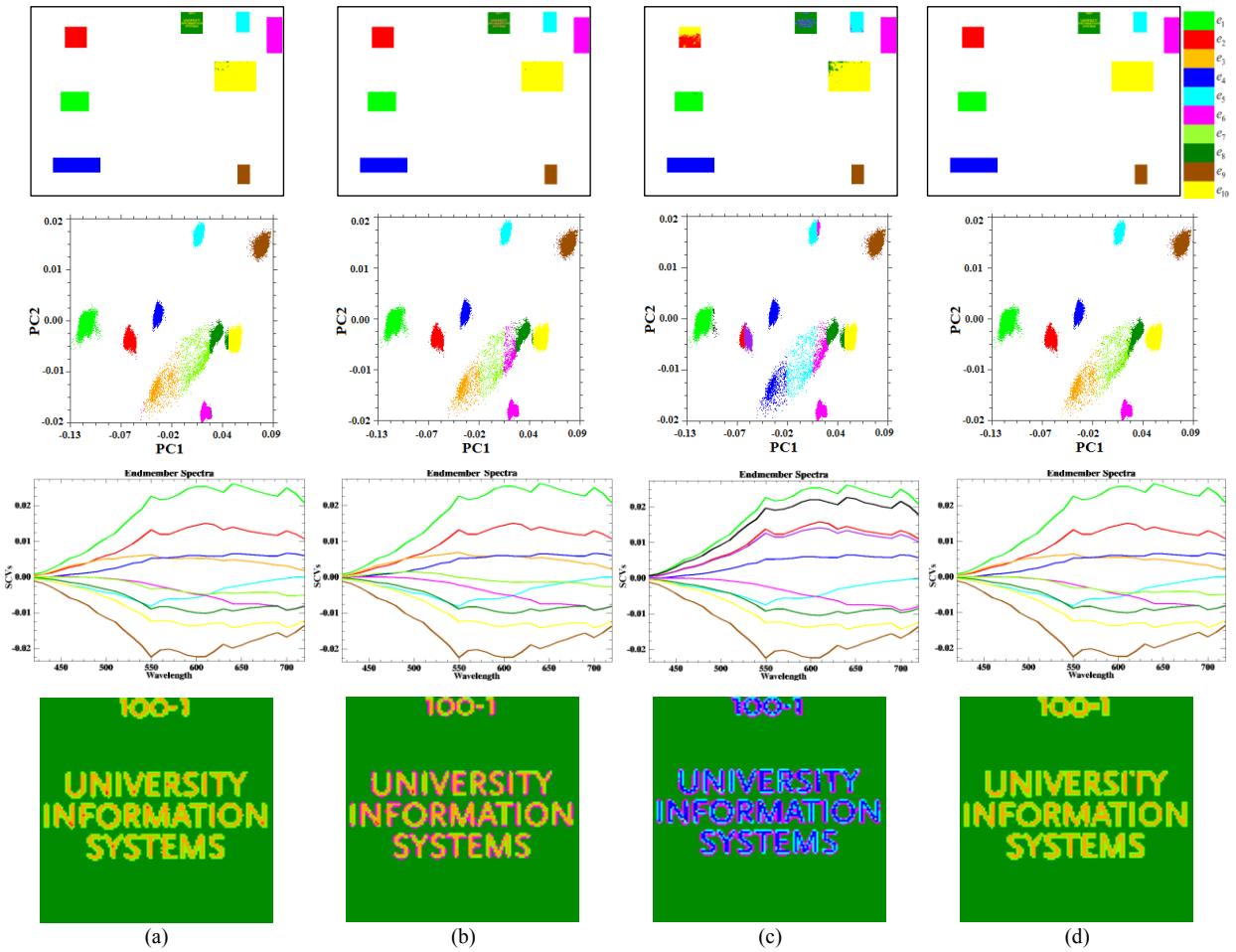

(a) (b) (c) (d)

Fig.10 CD results obtained on the simulated HS data set. Results provided by: (a) the proposed method, (b) *k*-means, and (c) FCM, (d) ground truth. From up to down, each row represents: (1) CD maps (or reference map); (2) 2-D scatterplots of change classes in the feature space; (3) SCV signatures of detected changes; (4) a subset from results in (1).

Let us now analyze one of the three simulated cases in greater detail (see Section IV Fig.7). In this case, the complete tree has a structure with 3 levels and 14 nodes, where 10 of them are leaf nodes identified as change endmembers. The CD maps obtained by the proposed method and the reference ones are shown in the first row of Fig.10. Fig.10 (a)-(c) reports the results of the proposed method, the reference *k*-means and FCM, respectively. Fig.10 (d) shows the reference map. Each color corresponds to a specific detected change endmember, whereas the unchanged pixels are in white. In the second row, 2-D scatterplots of the detected change classes are shown in the feature space of first two PCs extracted from pixels in Ω_c. The spectral behaviors of the change endmembers in the SCV domain are presented in row 3. Tiles extracted from the whole CD maps are illustrated and further compared in row 4. Accuracies and error indices obtained according to the reference data are summarized in TABLE II.

TABLE II
ENDMEMBER AND KAPPA ACCURACY, NUMBER OF DETECTION ERRORS AND MULTI-CLASS BHATTACHARYYA DISTANCE OBTAINED BY THREE CONSIDERED METHODS ON ONE OF THE SIMULATED DATA SETS.

Method	Endmember accuracy (%)										κ	Tot. errors (pixel)	Multi-class *Bhattacharyya* distance
	e_1	e_2	e_3	e_4	e_5	e_6	e_7	e_8	e_9	e_{10}			
PCA *k*-means	100.00	99.97	88.56	100.00	99.99	91.37	39.34	98.15	100.00	97.42	0.9770	1367	5.49
PCA FCM	99.77	57.30	0.00	100.00	97.10	97.20	0.00	97.92	100.00	94.30	0.9007	2218	4.93
Proposed method	100.00	99.93	92.10	100.00	100.00	99.94	86.60	99.46	100.00	99.07	0.9933	650	6.22

As we can see from Fig.10, the proposed method detected the expected changes on this simulated data set accurately. In particular, it identified properly the change classes in a hierarchical way, and it was not affected by the problem on minority classes. The subtle changes with small amount of pixels (e.g., change of letters and their edges) were also detected in a precise way (see row 4 in Fig.10). On the contrary, despite the conventional *k*-means and FCM received as input the true number of change endmembers, their results were less accurate. This demonstrates the advantages of using the hierarchical analysis structure. A visual comparison of scatterplots confirms the better results produced by the

proposed method with respect to the other techniques. The two reference methods obtained in overall good performances, but showed a higher error rate for some change endmembers (e.g., e_6 is confused with e_7 in *k*-means; and e_3 with e_4 in FCM). By comparing the SCV signatures of changes detected by the three methods (Fig.10 row 3 (a)-(c)) with the one of reference change map (Fig.10 row 3 (d)), we can observe: 1) higher similarity between results of the proposed method and the reference spectra; and 2) different kinds of change (i.e., change endmembers) have discriminable spectral behaviors in the SCV domain (see row 3 (a) in Fig.10), thus indicating the effectiveness of the proposed method in separating change information. The reference techniques detected some wrong change endmembers. For example, in the result of the FCM there are two couples of change endmembers with very similar spectral signatures. The first couple is represented by red and purple signatures, and the second is given by green and sienna signatures in Fig.10 (c) row 3. These changes were wrongly detected by the FCM method even by fixing the correct number of input classes.

The above analysis is confirmed by the numerical results in TABLE II. We can observe that: 1) the proposed hierarchical method outperformed reference approaches in terms of kappa accuracy and number of errors. The kappa accuracy is the highest among the three (i.e., 0.9933 compared to 0.9770 for *k*-means and 0.9007 for FCM). The total error of the proposed method (i.e., 650 pixels) is significantly smaller than the ones of reference methods (i.e., 1367 pixels for *k*-means and 2218 pixels for FCM); 2) on each single change endmember, the two reference approaches resulted in significant errors (both omission and commission), whereas the proposed method exhibits the highest accuracy. This further confirms the difficulty of the reference methods to directly identify endmembers; 3) the multi-class Bhattacharyya distance values indicate that the proposed approach achieves the highest class separability (i.e., 6.22) with respect to the two clustering methods (i.e., 5.49 in *k*-means and 4.93 in FCM, respectively).

B. Hyperion satellite images of an irrigated agricultural area

In this case the threshold T_σ was set to 0.13. The proposed method detected 15 change endmembers as leaf nodes in the hierarchical tree, which includes 4 levels and 20 nodes. Fig.11 illustrates CD results obtained by (a) the proposed hierarchical method, (b) the *k*-means, and (c) the FCM. From row 1 to row 3 the figure shows the CD maps, the 2-D scatterplots in the two-dimensional feature space (i.e., the first two PCs extracted from pixels in Ω_c), and the SCV signatures of all the detected changes, respectively. For the proposed hierarchical approach the 15 change endmembers are represented with different colors, whereas the no-change pixels are in white. For the two reference methods, the change clusters are also shown in different colors, but it is not possible to establish a direct correspondence among the legend given for the proposed method in Fig.11, and the colors used for the reference methods. Also in this case the number of clusters for the *k*-means and the FCM was fixed on the basis of the result produced by the proposed technique.

The proposed hierarchical CD approach obtained satisfactory results detecting change endmembers (validated by the detailed photointerpretation) and separating them according to the defined spectral homogeneity level. In greater detail, we can observe that: 1) The proposed method detected change endmembers due to the hierarchical analysis. On the contrary, the other two reference methods (that identify all the changes in a single step) ignore the intrinsic hierarchy of the change information in HS images. This increased the errors in the detection of change classes. (see also Fig.11 row 1, where the proposed method detects changes with a higher homogeneity than the two reference methods). 2) All the considered methods are able to discriminate multiple changes, but with different performance on the change separability of change endmembers. The multi-class Bhattacharyya distance values were 4.12 (proposed method), 3.78 (*k*-means) and 3.65 (FCM). The proposed method obtained the highest separability among all the detected change endmembers. 3) The generated spectra of change endmembers point out the spectral differences in the SCV domain, which illustrate the change

separability of the different considered methods.

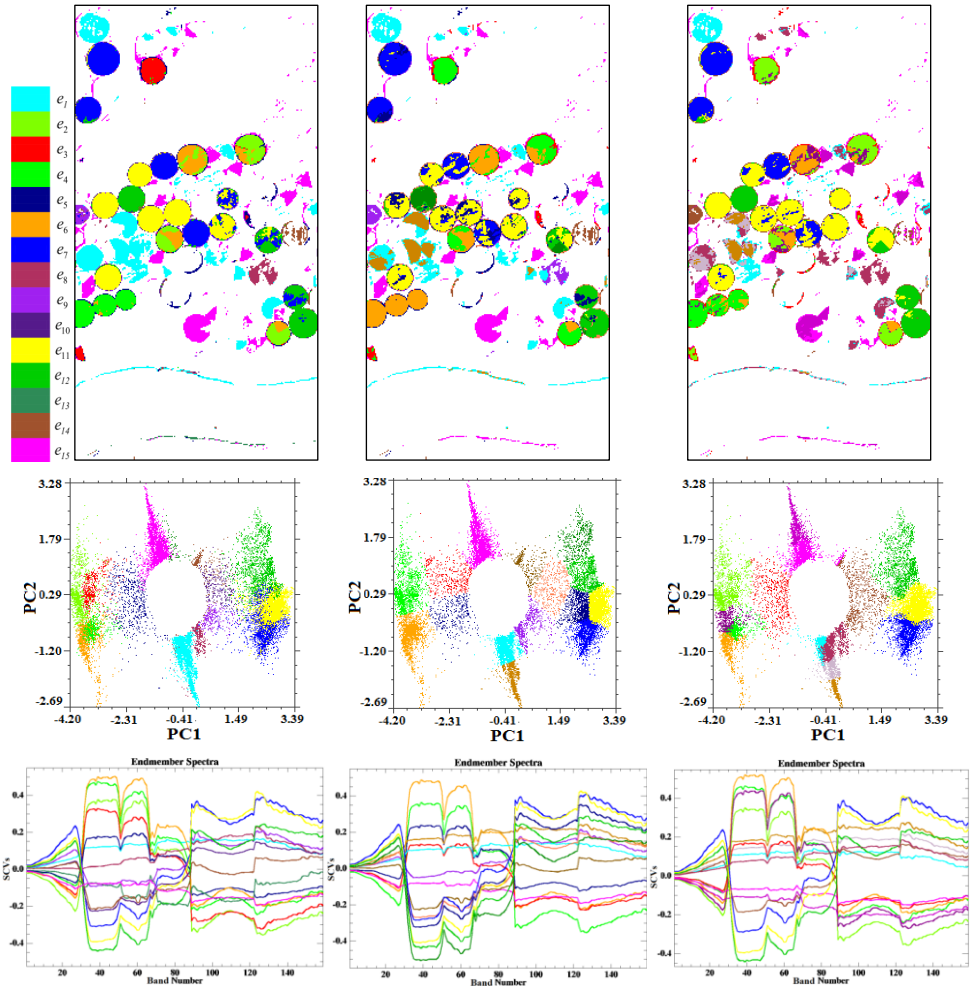

Fig.11 CD results obtained on the real Hyperion HS images on an agricultural area. Results provided by (a) the proposed method, (b) the *k*-means, and (c) the FCM. From row 1 to row 3: (1) change-detection maps; (2) 2-D scatterplots of all change classes in the feature space by using the first two PCs computed on pixels in Ω_c; (3) spectra of the detected changes in the SCV domain. The legend only applies to the proposed method results.

C. Hyperion images of a wetland agricultural area

On the third data set we carried out the same experiments as for the previous one. The threshold T_σ was set to 0.15. The hierarchical tree structure consisted of 5 levels with 27 nodes, where 17 change endmembers were detected according to 17 leaf nodes. As we can see from the CD results, in this case the proposed method also obtained satisfactory results. A qualitative analysis points out that the change endmembers were properly detected (see Fig.12). The multi-class Bhattacharyya distances for the three

methods were 3.89 (proposed method), 3.49 (*k*-means) and 3.30 (FCM). Also in this case, the proposed hierarchical method achieved the highest multi-class separability, whereas the *k*-means and FCM resulted in a lower separability, despite the two reference methods are driven by the number of endmembers automatically detected by the proposed method.

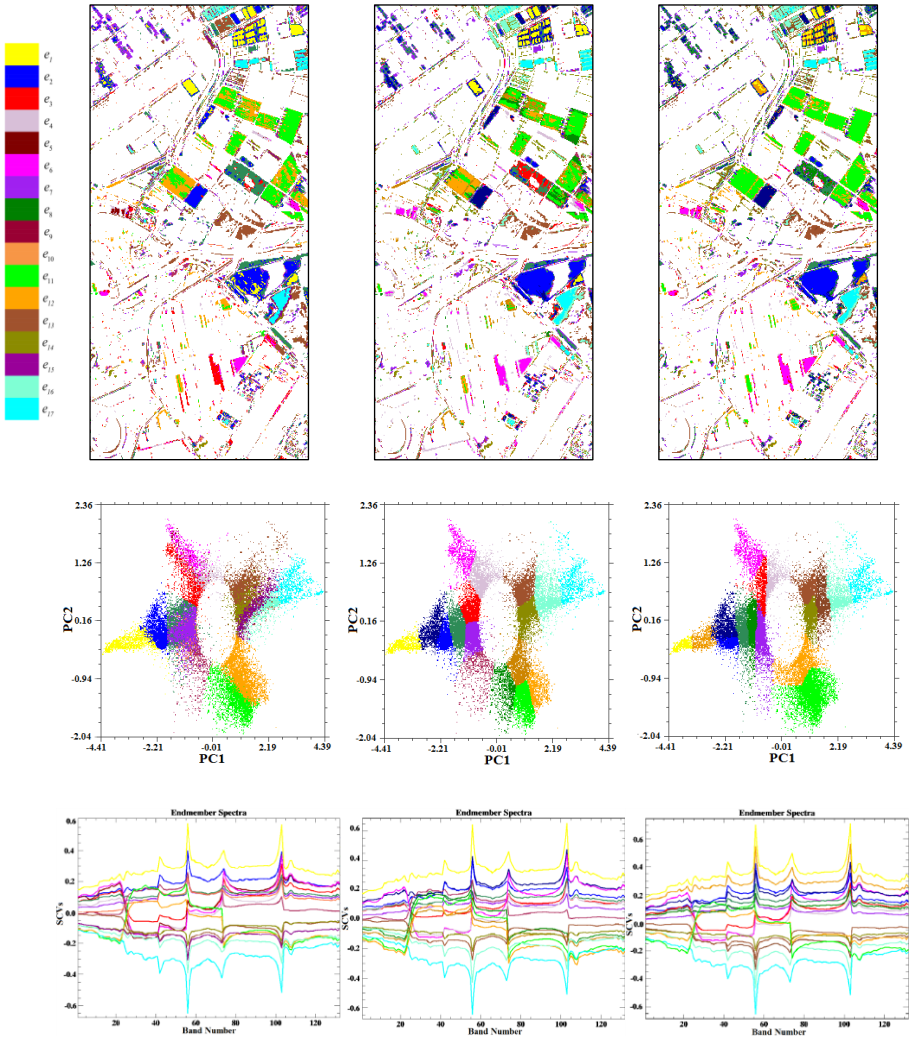

(a) (b) (c)

Fig.12 CD results obtained on the real Hyperion images on a coastal wetland agricultural area in China. Results provided by (a) the proposed method, (b) the *k*-means, and (c) the FCM. From row 1 to row 3: (1) CD maps; (2) 2-D scatterplots of all change classes in feature space by using first two PCs computed on pixels in Ω_c; (3) SCV spectra of the detected changes (17 changes in different colors, no-change class in white). The legend only applies to the proposed method results.

VI. DISCUSSION AND CONCLUSION

This paper analyzed and discussed the change-detection problem in multitemporal hyperspectral images. By taking into account the intrinsic complexity of the HS data, a proper definition of the concept of "change" in HS images is given and the concept of change endmembers is introduced. A novel hierarchical spectral change analysis approach has been proposed to detect and identify multiple-change information in an unsupervised way. Accordingly, the change endmembers are detected hierarchically by analyzing the spectral properties in the SCV domain. Moreover, the proposed hierarchical analysis can identify the discriminable spectral change endmembers from coarse to fine level leading to a better model, whereas the reference methods are based on a single step of processing only. Since in the CD-HS case, the number of change endmembers is usually high, those methods are generally not able to correctly identify all of them. Satisfactory results obtained on both the simulated and real multitemporal HS remote sensing images confirmed the effectiveness of the proposed CD method.

The main contributions of this work are as follows: 1) Analysis and definition of the concept of changes in HS images, proposal of a technique for addressing the challenging multiple-change detection problem in HS images, by considering the difference of spectral change behaviors in the SCV domain at different spectral detail scales; and 2) proposal of an approach that models the detection of multiple changes in a hierarchical way, to identify the change information and separate different kinds of changes (major change, subtle change and finally change endmembers) according to their spectral difference. In this way, we progressively decompose the complex problem into several specific sub-problems, focusing on each single portion of the multiple-change information. This makes it possible to discover the difference among similar changes by decreasing the difficulty of detection. Moreover, the proposed approach is designed in an unsupervised way, thus it fits most of actual applications, for which often the ground truth is not available.

A minor limitation of the proposed method consists in the use of CVA for the pseudo binary CD step. By computing the magnitude of SCVs, small portions of the change information might be lost after

compression, thus causing missed alarms in the final CD map. Although a proper setting of margin δ may limit this problem, the high dimensionality of HS data may still produce errors. Another issue to consider is the tuning of the threshold value (i.e., T_σ), which impacts on the final number of the output change endmembers. T_σ should be fixed in order to tune the sensitivity of the method according to the end-user requirements. This can be done considering the fact that T_σ has a clear physical meaning with respect to the sensitivity of the method. Although additional investigations should be done to define a possible automatic technique for the detection of the optimal threshold, we point out that the selection of T_σ is more simple and reliable than the selection of the number of endmembers in standard clustering methods.

As future development of this work, the robustness of the proposed method will be tested on the available multitemporal HS images showing differences in illumination conditions and no real change. Moreover, we plan to: i) consider in the proposed technique also the spatial information in order to increase the robustness and the accuracy of the CD results; ii) define a reliable automatic technique for the detection of the above mentioned threshold; iii) define alternative methods for the identification of change endmembers; iv) investigate the CD-HS problem on data sets for which an exhaustive ground truth is available.

ACKNOWLEDGEMENTS

This work was carried out in the framework of the project “Very high spatial and spectral resolution remote sensing: a novel integrated data analysis system”, funded by the Italian Ministry of Education, University and Research (Ministero dell'Istruzione, dell'Università e della Ricerca - MIUR) as a research program of relevant national interest (Programmi di Ricerca di Rilevante Interesse Nazionale – PRIN 2012).

APPENDIX

The notation used in the paper is listed in TABLE III.

TABLE III
NOTATION USED IN THE PAPER.

Symbol	Description	Symbol	Description
$\boldsymbol{X_t}$	HS images acquired at time t	ρ_i	SCV magnitude of $\boldsymbol{x_i}$
P	Length of image $\boldsymbol{X_t}$	L_d	d-th level of the hierarchy tree structure
Q	Width of image $\boldsymbol{X_t}$	D	Depth of the tree
$\boldsymbol{X_D}$	Spectral change vectors (SCVs)	$\boldsymbol{S}_{\Omega_c}$	Reference spectrum calculated by averaging all $\boldsymbol{x_i} \in \Omega_c$
$\boldsymbol{x_i}$	SCV with spatial position i in $\boldsymbol{X_D}$	$\vartheta(\boldsymbol{x_i}, \boldsymbol{S}_{\Omega_c})$	Spectral angle distance between $\boldsymbol{x_i}$ and $\boldsymbol{S}_{\Omega_c}$
Ω_c	Set of change classes	$\sigma_{\vartheta_{\Omega_c}}$	Standard deviation value of $\vartheta(\boldsymbol{x_i}, \boldsymbol{S}_{\Omega_c})$
ω_{C_K}	K-th detected major change in Ω_c	$\boldsymbol{P}$	Image with selected M (M < B) PCs
Ω_e	Set of change endmembers	$\boldsymbol{P_i}$	Vector with spatial position i in $\boldsymbol{P}$
e_E	E-th change endmember	M	Number of selected PCs
E	Number of change endmembers	k	Number of major changes in Ω_c
e_n	Endmember of no-change class	U	Range of number k
ω_n	Class of no-change	k_0	Initial number of k (i.e., lower bound of U)
ρ	Magnitude of SCVs	t	A constant value to control the upper bound of U
B	Number of the spectral channels (bands) of the considered images	$\varphi(\boldsymbol{P_i})$	Compressed change direction of $\boldsymbol{P_i}$
T_ρ	Magnitude threshold for separating the Ω_c and ω_n	$\boldsymbol{S}_{e_j}$	Reference spectrum of endmember $e_j \in \{\Omega_e, e_n\}$
δ	A margin value on the threshold	$B_{\alpha,\beta}$	Bhattacharyya distance between e_α and e_β
$h(\rho)$	The histogram of ρ	$\boldsymbol{\mu}_\alpha$	Mean vector of e_α
Ω_u	Set of uncertain pixels	$\boldsymbol{\Gamma}_\alpha$	Covariance matrix of e_α

REFERENCES

[1] L. Bruzzone, F. Bovolo, "A Novel Framework for the Design of Change-Detection Systems for Very-High-Resolution Remote Sensing Images," *Proceedings of the IEEE*, no.99, pp.1-22, 2012.

[2] P.R. Coppin, M. Bauer, "Digital change detection in forest ecosystems with remote sensing imagery," *Remote Sens. Reviews*, 13, pp.207-304, 1996.

[3] M. K. Ridd, J. J. Liu, "A comparison of four algorithms for change detection in an urban environment," *Remote Sens. Environ.*, vol.63, no.2, pp.95-100, 1998.

[4] X. Yang, L. Chen, "Using multi-temporal remote sensor imagery to detect earthquake-triggered landslides," *Inter. J. of Applied Earth Obs. and Geosci*., vol.12, no.6, pp.487-495, 2010.

[5] A. Singh, "Digital change detection techniques using remotely sensed data," *Int. J. Remote Sens.*, vol.10, no. 6, pp. 989-1003, 1989.

[6] D. Lu, P. Mausel, E. Brondi'Zio, E. Moran, "Change detection techniques," *Int. J. Remote Sens.*, vol.25, no.12, pp.2365-2407, 2004.

[7] P.R. Coppin, I. Jonckheere, K. Nackaerts, B. Muys, "Digital change detection methods in ecosystem monitoring: a review," *Int. J. Remote Sens.*, vol. 25, no. 9, pp.1565-1596, 2004.

[8] F. Bovolo, "A Multilevel Parcel-Based Approach to Change Detection in Very High Resolution Multitemporal Images," *IEEE Geosci. Remote Sens. Lett.*, vol.6, no.1, pp.33-37, 2009.

[9] S. Marchesi, F. Bovolo, L. Bruzzone, "A Context-Sensitive Technique Robust to Registration Noise for Change Detection in VHR Multispectral Images," IEEE Transactions on Image Processing, *IEEE Trans. Geosci. Remote Sens.*,

vol.19, no.7, pp.1877-1889, 2010.
[10] M. Frank, M. Canty, “Unsupervised Change Detection for Hyperspectral Images,” *In 12th JPL Airborne Earth Science Workshop*, pp.63-72, 2003.
[11] S. Liu, L. Bruzzone, F. Bovolo, P. Du, “Unsupervised hierarchical spectral analysis for change detection in hyperspectral images,” *Proc. 4th WHISPERS*. Shanghai, China, 4-7 June, 2012.
[12] A. Chakrabarti, T. Zickler, "Statistics of Real-World Hyperspectral Images," in *Proceedings of the IEEE Conference on Computer Vision and Pattern Recognition (CVPR)*, pp.193-200, 2011.
[13] R. J. Radke, S. Andra, O. Al-Kofahi, B. Roysam, “Image change detection algorithms: a systematic survey,” *IEEE Trans. Image Process.*, vol.14, no.3, pp. 294-307, 2005.
[14] L. Castellana, A. D’Addabbo, G. Pasquariello, “A composed supervised/unsupervised approach to improve change detection from remote sensing,” *Pattern Recogn. Lett.,* vol.28, no.4, pp.405-413, 2007.
[15] V.P. Soares, R. M. Hoffer, “Eucalyptus forest change classification using multi-data Landsat TM data,” *Proceedings, SPIE*, 2314, pp.281-291, 1994.
[16] L. Bruzzone, S.B. Serpico, "An iterative technique for the detection of land-cover transitions in multitemporal remote-sensing images," *Geoscience and Remote Sensing, IEEE Transactions on*, vol.35, no.4, pp.858-867, Jul 1997.
[17] H. Nemmour, Y. Chibani, “Multiple support vector machines for land cover change detection: An application for mapping urban extensions,” *ISPRS J Photogramm*, vol.61, no.2, pp.125-133, 2006.
[18] L. Bruzzone and R. Cossu, “A multiple cascade-classifier system for a robust a partially unsupervised updating of land-cover maps,” *IEEE Trans. Geosci. Remote Sens.*,vol. 40, no. 9, pp. 1984–1996, Sep. 2002.
[19] B. Demir, F. Bovolo, L. Bruzzone, “Detection of land-cover transitions in multitemporal remote sensing images with active-learning-based compound classification,” *IEEE Trans. Geosci. Remote Sens.*, vol.50, no.5, pp.1930-1941, 2012.
[20] K. Chen, Z. Zhou, C. Huo, X. Sun, K. Fu, “A Semisupervised Context-Sensitive Change Detection Technique via Gaussian Process,” *IEEE Geosci. Remote Sens. Lett.*, vol.10, no.2, pp.236-240, 2013.
[21] G. F. Hughes, “On the mean accuracy of statistical pattern recognizers,” *IEEE Trans. on Inf. Theory*, IT-14, pp.55-63, 1968.
[22] L. Bruzzone, S. B. Serpico, “Detection of changes in remotely-sensed images by the selective use of multi-spectral information,” *Int. J. Remote Sens.,* vol.18, no.18, pp.3883-3888, 1997.
[23] L. Bruzzone, D. Fernandez Prieto, “A minimum-cost thresholding technique for unsupervised change detection,” *Int. J. Remote Sens.,* vol.21, no.18, pp.3539-3544, 2000.
[24] L. Bruzzone, D. Fernandez Prieto, “Automatic analysis of the difference image for unsupervised change detection,” *IEEE Trans. Geosci. Remote Sens.*, vol.38, no.3, pp.1170-1182, 2000.
[25] T. Celik, “Change detection in satellite images using a genetic algorithm approach,” *IEEE Geosci. Remote Sens. Lett.*, vol.7, no. 2, pp.386-390, 2010.
[26] P. Du, S. Liu, P. Gamba, K. Tan, J. Xia, “Fusion of Difference Images for Change Detection over Urban Areas,” *IEEE J. Sel. Top. in Applied Earth Obs. and Remote Sens.*, vol.5, no.4, pp.1076-1086, 2012.
[27] P. Du, S. Liu, J. Xia, Y. Zhao, “Information fusion techniques for change detection from multi-temporal remote sensing images,” *Information Fusion*, vol.14, no.1, pp.19-27, 2013.
[28] S. Le Hegarat-Mascle, R. Seltz, “Automatic change detection by evidential fusion of change indices,” *Remote Sens. Environ.*, vol.91, no.3-4, pp. 390-404, 2004.
[29] T. Celik, “Unsupervised Change Detection in Satellite Images Using Principal Component Analysis and k-Means Clustering,” *IEEE Geosci. Remote Sens. Lett.*, vol.6, no.4, pp.772-776, 2009.
[30] A. Ghosh, N. S. Mishra, S. Ghosh, “Fuzzy clustering algorithms for unsupervised change detection in remote sensing images,” *Information Sciences*, vol.181, no.4, pp.699-715, 2013.
[31] J. Zhong, R. Wang, “Multi-temporal remote sensing change detection based on independent component analysis,” *Int. J. Remote Sens.,* vol.27, no.10, pp.2055-2061, 2006.
[32] M. J. Canty, A. A. Nielsen, “Visualization and unsupervised classification of changes in multispectral satellite imagery,” *Int. J. Remote Sens.,* vol.27, no.18, pp.3961-3975, 2006.
[33] A.A. Nielsen, K. Conradsen, J. J. Simpson, “Multivariate alteration detection (MAD) and MAF postprocessing in multispectral, bitemporal image data: New approaches to change detection studies,” *Remote Sens Environ.*, vol.64, no.1, pp.1-19, 1998.
[34] F. Bovolo, S. Marchesi, L. Bruzzone, “A framework for automatic and unsupervised detection of multiple changes in multitemporal images,” *IEEE Trans. Geosci. Remote Sens.*, vol.50, no.6, pp.2196-2212, 2012.
[35] F. Bovolo, L. Bruzzone, “An adaptive thresholding approach to multiple-change detection in multispectral images,” *IEEE Int. Geosci. Remote Sens. Symp.,* Vancouver, BC, 233-236, 2011.
[36] F. Bovolo, L. Bruzzon*e,* "A Theoretical Framework for Unsupervised Change Detection Based on Change Vector Analysis in the Polar Domain," *Geoscience and Remote Sensing, IEEE Transactions on* , vol.45, no.1, pp.218-236, 2007

[37] A. Schaum, A. Stocker, "Hyperspectral change detection and supervised matched filtering based on covariance equalization," *Proc. SPIE*, 5425, pp.77-90, 2004.
[38] A. Schaum, A. Stocker, "Long-interval chronochrome target detection," *Int. Symp. Spectral Sens. Res.* 1997.
[39] A.A. Nielsen, "The Regularized Iteratively Reweighted MAD Method for Change Detection in Multi- and Hyperspectral Data," *IEEE Trans. on Image Proc.*, vol.16, no.2, pp.463-478, 2007.
[40] V. Ortiz-Rivera, M. Vélez-Reyes, B. Roysam, "Change detection in hyperspectral imagery using temporal principal components," *Proc. SPIE, Algorithms and Technologies for Multispectral, Hyperspectral, and Ultraspectral Imagery XII.* vol. 6233, pp.623312, 2006.
[41] S. Adar, G. Notesco, A. Brook, Livne, et al. "Change detection over Sokolov open-pit mining area, Czech Republic, using multi-temporal HyMAP data (2009-2010)," *Proc. SPIE 8180, Image and Signal Processing for Remote Sensing XVII, 81800T*. 2011.
[42] Y. Z. Du, C. I. Chang, H. Ren, C.C. Chang, J.O. Jensen, et al. "New hyperspectral discrimination measure for spectral characterization," *Opt. Eng*. vol.43, no.8, pp.1777-1786, 2004.
[43] K. Vongsy, M.J. Mendenhall, "A comparative study of spectral detectors," *Proc. 3rd WHISPERS*. Lisbon, Portugal. 6-9 June 2011. 1-4, 2011.
[44] Q. Du, L. Wasson, R. King, "Unsupervised linear unmixing for change detection in multitemporal airborne hyperspectral imagery," *Int. Workshop on MultiTemp*, 136-140, 16-18 May, 2005.
[45] Q. Du, N. Younan, R. King, "Change Analysis for Hyperspectral Imagery," *Int. Workshop on MultiTemp*, 1-4, 18-20 July, 2007.
[46] J. Meola, M.T. Eismann, R.L. Moses, J.N. Ash, "Detecting Changes in Hyperspectral Imagery Using a Model-Based Approach," *IEEE Trans. Geosci. Rem. Sens.*, vol.49, no.7, pp. 2647-2661, 2011.
[47] Q. Du, "A new method for change analysis of multi-temporal hyperspectral images," *Proc. 4td WHISPERS*. Shanghai, China, 4-7 June, 2012.
[48] K. Vongsy, M.J. Mendenhall, M.T. Eismann, G. L. Peterson, "Removing parallax-induced changes in Hyperspectral Change Detection," *IEEE Int. Geosci. and Remote Sens. Symp*. pp. 2012-2015, 22-27 July 2012, 2012.
[49] J. Meola, M.T. Eismann, K.J. Barnard, R.C. Hardie, "Analysis of hyperspectral change detection as affected by vegetation and illumination variation," *Proc. SPIE*, 6565, 65651S-1–65651S-12. 2007.
[50] M. T. Eismann, J. Meola, A. Stocker, S. Beaven, A. Schaum, "Hyperspectral change detection in the presence of diurnal and seasonal variations," *IEEE Trans. Geosci. Remote Sens.*, vol.46, no.1, 237-249, 2008.
[51] M. Dalponte, L. Bruzzone, L. Vescovo and D. Gianelle, "The role of spectral resolution and classifier complexity in the analysis of hyperspectral images of forest areas," *Remote Sensing of Environment*, Vol. 113, pp. 2345–2355, November 2009.
[52] C.M. Bishop, *Pattern Recognition and Machine Learning*, Springer-Verlag New York,2006.
[53] A. Plaza, P. Martinez, R. Perez, J. Plaza, "A quantitative and comparative analysis of endmember extraction algorithms from hyperspectral data," *IEEE Trans. Geosci. Remote Sens.*, vol.42, no.3, pp.650-663, 2004.
[54] D. Pelleg, A. W. Moore. "X-means: Extending K-means with Efficient Estimation of the Number of Clusters," In *Proceedings of the Seventeenth International Conference on Machine Learning* (ICML '00), Pat Langley (Ed.). Morgan Kaufmann Publishers Inc., San Francisco, CA, USA, 727-734, 2000.
[55] T. Ishioka, "An expansion of x-means for automatically determining the optimal number of clusters - Progressive iterations of k-means and merging of the clusters," *In: IASTED International Conference on Computational Intelligence*, pp. 91-96, 2005.
[56] X. Hu, L. Xu, "Investigation on several model selection criteria for determining the number of cluster," *Neural Inform. Proces. Lett. and Reviews*, vol.4, pp. 2004, 2004.
[57] S. Tu, L. Xu, "A theoretical investigation of several model selection criteria for dimensionality reduction," *Pattern Recognition Letters*, vol. 33, no. 9, pp. 1117-1126, 2012.
[58] Real-World Hyperspectral Images Database. [Online]. Available: http://vision.seas.harvard.edu/hyperspec/.
[59] Earth science data archives of U.S. Geological Survey (USGS). [Online]. Available: http://earthexplorer.usgs.gov/.
[60] R. Beck. "EO-1 User Guide," Version 2.3, 15 July 2003. Available: http://eo1.usgs.gov.

Sicong Liu received the B.Sc. degree in Geographical Information System and the M.E. degree in photogrammetry and remote sensing from China University of Mining and Technology, China, in 2009 and 2011, respectively. He is currently a Ph.D. student with the Remote Sensing Laboratory, Department of Information Engineering and Computer Science, University of Trento, Italy. His research interests include multitemporal data processing, change detection, spectral signal analysis in multispectral /hyperspectral images.

He serves as a reviewer for several international remote sensing journals, including *IEEE Transactions on Geoscience and Remote Sensing*, *IEEE Journal of Selected Topics in Applied Earth Observation and Remote Sensing*, *IEEE Geoscience and Remote Sensing Letters*, *Remote Sensing*, etc.

Lorenzo Bruzzone (S'95–M'98–SM'03–F'10) received the Laurea (M.S.) degree in electronic engineering (summa cum laude) and the Ph.D. degree in telecommunications from the University of Genoa, Italy, in 1993 and 1998, respectively.

He is currently a Full Professor of telecommunications at the University of Trento, Italy, where he teaches remote sensing, radar, pattern recognition, and electrical communications. Dr. Bruzzone is the founder and the director of the Remote Sensing Laboratory in the Department of Information Engineering and Computer Science, University of Trento. His current research interests are in the areas of remote sensing, radar and SAR, signal processing, and pattern recognition. He promotes and supervises research on these topics within the frameworks of many national and international projects. Among the others, he is the Principal Investigator of the *Radar for icy Moon exploration (RIME)* instrument in the framework of the *JUpiter ICy moons Explorer (JUICE)* mission of the European Space Agency. He is the author (or coauthor) of 150 scientific publications in referred international journals (101 in IEEE journals), more than 215 papers in conference proceedings, and 16 book chapters. He is editor/co-editor of 11 books/conference proceedings and 1 scientific book. His papers are highly cited, as proven form the total number of citations (more than 9620) and the value of the h-index (51) (source: Google Scholar). He was invited as keynote speaker in 24 international conferences and workshops. Since 2009 he is a member of the Administrative Committee of the IEEE Geoscience and Remote Sensing Society.

Dr. Bruzzone ranked first place in the Student Prize Paper Competition of the 1998 IEEE International Geoscience and Remote Sensing Symposium (Seattle, July 1998). Since that time he was recipient of many international and national honors and awards. Dr. Bruzzone was a Guest Co-Editor of different Special Issues of international journals. He is the co-founder of the IEEE International Workshop on the Analysis of Multi-Temporal Remote-Sensing Images (MultiTemp) series and is currently a member of the Permanent Steering Committee of this series of workshops. Since 2003 he has been the Chair of the SPIE Conference on Image and Signal Processing for Remote Sensing. Since 2013 he has been the founder Editor-in-Chief of the IEEE GEOSCIENCE AND REMOTE SENSING MAGAZINE. Currently he is an Associate Editor for the IEEE TRANSACTIONS ON GEOSCIENCE AND REMOTE SENSING and the CANADIAN JOURNAL OF REMOTE SENSING. Since 2012 he has been appointed *Distinguished Speaker* of the IEEE Geoscience and Remote Sensing Society.

Francesca Bovolo (S'05–M'07-SM'13) received the "Laurea" (B.S.), the "Laurea Specialistica" (M.S.) degrees in telecommunication engineering (*summa cum laude*) and the Ph.D. in Communication and Information Technologies from the University of Trento, Italy, in 2001, 2003 and 2006, respectively where she has been a research fellow until June 2013.

She is the founder and the head of the Remote Sensing for Digital Earth unit at Fondazione Bruno Kessler (FBK), Trento, Italy and a member of the Remote Sensing Laboratory (RSLab) in Trento. Her main research activity is in the area of remote-sensing image processing. Her interests are related to multitemporal remote sensing image analysis and change detection in multispectral, hyperspectral and SAR images, and very high resolution images, in particular. She conducts research on these topics within the context of several national and international projects. She is a referee for several international journals.

Dr. Bovolo ranked first place in the Student Prize Paper Competition of the 2006 *IEEE International Geoscience and Remote Sensing Symposium* (Denver, August 2006). Since January 2011 she is an associate editor of the *IEEE Journal of Selected Topics in Applied Earth Observations and Remote Sensing*. She has been guest editor for the Special Issue on "Analysis of Multitemporal Remote Sensing Data" of the *IEEE Transactions on Geoscience and Remote Sensing*. She is the Technical Chair of the Sixth International Workshop on the Analysis of Multi-temporal Remote-Sensing Images (MultiTemp 2011). From 2006 to 2013, she has served on the Scientific Committee of the SPIE International Conference on "Signal and Image Processing for Remote Sensing". Since 2014 she is co-chair of the same conference. Since 2012 she is a member of the international program committee of the conference on *Pattern Recognition Applications and Methods.* She has served on the Scientific Committee of the *IEEE Fourth and Fifth International Workshop on the Analysis of Multi-Temporal Remote Sensing Images (MultiTemp 2007 and 2009)* and of the *IEEE GOLD Remote Sensing Conference* in 2010, 2012, and 2014.

Peijun Du (M'07-SM'12) received the B.S. and Ph.D. degrees in Geomatics engineering and cartography and geographic information system from China University of Mining and Technology, Xuzhou, China, in 1997 and 2001, respectively. Currently, he is a Professor of photogrammetry and remote sensing at the Department of Geographical Information Science, Nanjing University, Nanjing, China.

From 2002 to 2004, he was a postdoctoral fellow with the Lab of Pattern Analysis & Machines Intelligence, Institue of Image Processing and Pattern Recognition, Shanghai Jiaotong University (SJTU), Shanghai, China. During 2006 to 2007, he was a visiting scholar at the University of Nottingham, Nottingham, U.K.

His research interests include remote sensing image processing and pattern recognition, remote sensing applications, hyperspectral remote sensing information processing, multi-source geospatial information fusion and spatial data handling, integration and applications of geospatial information technologies, and environmental information science (environmental informatics). He is the author of nine books in Chinese and more than 100 research articles about remote sensing and geospatial information processing and applications.

Dr. Du was the Co-chair of the Technical Committee, *URBAN 2009* (*the 5th IEEE GRSS/ISPRS Joint Workshop on Remote Sensing and Data Fusion over Urban Areas*), and the Co-chair of the local organizing committee of *JURSE 2009*. He also served as the member of scientific committee or local organizing committee of other international conferences, for example, *Accuracy 2008*, *ACRS 2009*, *WHISPERS 2010*, *2011* and *2012*, *URBAN 2011*, *MultiTemp 2011*, and *ISDIF 2011*. He is a member of *International Society of Environment Information Science* and *IEEE GRSS*, and a council member of *China Society for Image and Graphics (CSIG)*, *China Association for Remote Sensing Applications (CARSA)* and *Jiangsu Provincial Society of Remote Sensing and Geographic Information System*. He is also an Associate Editor for *IEEE Geoscience and Remote Sensing Letters*.